



Can low b value diffusion weighted imaging evaluate the character of cerebrospinal fluid dynamics?

Toshiaki Taoka¹ · Shinji Naganawa¹ · Hisashi Kawai¹ · Toshiki Nakane¹ · Katsutoshi Murata²

Received: 6 September 2018 / Accepted: 26 October 2018 / Published online: 8 November 2018
© Japan Radiological Society 2018

Abstract

Purpose We aimed to investigate whether low b value diffusion-weighted imaging (DWI) can show the change of cerebrospinal fluid (CSF) dynamics.

Materials and methods The subjects of this retrospective study consisted of patients with ventricular dilatation ($n = 50$) and controls ($n = 50$). The CSF signal intensity on the $b = 500$ s/mm² DWI was evaluated by a scoring method in the lateral, 3rd and 4th ventricles, the cerebral sulci and the Sylvian fissure. The signal void findings adjacent to the septum pellucidum were also evaluated.

Results The CSF signal intensities were significantly less in lateral ventricle and 3rd ventricle of the ventricular dilatation subjects. In controls, the score for the signal void in the Sylvian fissure showed a significant positive correlation with age. However, other areas did not show a significant correlation with age. The appearance of the characteristic signal void adjacent to the septum pellucidum showed a significant correlation with ventricular dilatation.

Conclusion Our current study suggests that the CSF signal intensity on the $b = 500$ s/mm² DWI may show the changes in CSF dynamics and might be useful to evaluate the overlook of CSF dynamics.

Keywords Diffusion-weighted image · Low b value · Ventricular dilatation · Cerebrospinal fluid dynamics · Septum pellucidum

Introduction

Following the development of diffusion imaging, various aspects of the central nervous system have been evaluated by MR-imaging techniques that assess diffusion [1–4]. In routine clinical practice, diffusion-weighted imaging (DWI) with a b value of 1000 s/mm² is preferred. This is because acute infarction can be well visualized at this b value and the effect of T2 ‘shine through’ is sufficiently suppressed. DWI with $b = 1000$ s/mm² is also useful for the evaluation of demyelinating disease or brain tumors [4–6]. The apparent diffusion coefficient (ADC) image is also useful to delineate diffusion alterations by excluding the effect of T2 shine

through. The ADC can be calculated by DWI with either $b = 0$ or $b = 1000$ s/mm²; however, DWI using multiple b values has been used to obtain accurate and stable ADC values that are insensitive to perfusion effects [7, 8]. For an accurate and stable ADC calculation, we use multiple b value DWI ($b = 0, 500$ and 1000 s/mm²) for daily clinical practice, and we generally utilize the $b = 1000$ s/mm² image as well as the $b = 0$ image. In contrast, usually, we do not use the $b = 500$ s/mm² image for the clinical diagnosis, because the contrast between acute infarction and normal tissue is not sufficient, and the interpretation of the signal intensity on the $b = 500$ s/mm² image is complicated by a larger effect of T2 shine through. In addition, the signal intensity from the cerebrospinal fluid (CSF) is not fully suppressed on the $b = 500$ s/mm² image and is not uniform, which makes clinical reading a challenge. Although the lower b value DWI is important as a source image for intra-voxel incoherent motion (IVIM) measurement [9–11], the independent use of the lower b value DWI for diagnoses in the brain has not been discussed in the previous literature.

✉ Toshiaki Taoka
ttaoka@med.nagoya-u.ac.jp

¹ Department of Radiology, Graduate School of Medicine, Nagoya University, 65 Tsurumai-cho, Showa-ku, Nagoya, Aichi 466-8550, Japan

² Siemens Japan K.K., 1-11-1 Osaki, Shinagawa-ku, Tokyo 141-0032, Japan

While making daily clinical reading, we found that the signal distribution of CSF on $b = 500 \text{ s/mm}^2$ images differs by the cases and there were several interesting findings. We found that there were differences in the signal distribution between the cases with and without ventricular dilatation. We also found that there curious beads like low signal areas along the septum pellucidum especially in the cases with severe ventricular dilatation cases, which is the secondary investigation purpose for the current study. From these observations, we considered that the signal distribution due to incomplete signal suppression of the CSF might contain information regarding CSF dynamics, despite the disadvantage of $b = 500 \text{ s/mm}^2$ images for clinical practice indicated above. Thus, the purpose for this study is to investigate if characteristics or alterations of CSF dynamics can be visualized and evaluated by the signal distribution on the $b = 500 \text{ s/mm}^2$ DWI.

Materials and methods

Subjects

This retrospective study was approved by our institutional review board. The subjects were enrolled from the image report server of our institute. The subjects were scanned on a single 1.5 T clinical scanner with a fixed DWI sequence described in the next section. We performed a text search on the image report server for “ventricular dilatation”. From the text search results, we included the cases in which Evans’ index is larger than 30%. We excluded cases with space occupying lesions larger than 2 cm diameter, cases with cerebral infarction larger than one cerebral gyrus, and traumatic brain damage cases larger than one cerebral gyrus, which can result in brain deformation. Thus, we obtained 51 consecutive cases, which were enrolled as the “ventricular dilatation group”. The ventricular dilatation group consisted of 26 males and 24 females, and a median age of 69 that ranged from 0 to 87 (1st decade: 5, 2nd decade: 6, 3rd decade: 1, 4th decade: 4, 5th decade: 3, 6th decade: 2, 7th decade: 8, 8th decade: 11, and 9th decade: 11). The underlying condition for the ventricular dilatation was as follows; brain atrophy: 23, aqueductal stenosis: 9, post chemotherapy: 4, hydrocephalus with unknown cause: 4, post-surgery: 3, Chiari anomaly: 3, post intraventricular hemorrhage: 2, meningitis: 2, achondroplasia: 1.

We also searched for reports, which do not contain “ventricular dilatation”. We excluded cases with space occupying lesions larger than 2 cm diameter, cases with cerebral infarction larger than one cerebral gyrus, and traumatic brain damage cases larger than one cerebral gyrus. Thus, we obtained 51 consecutive cases, which were enrolled as the “control group”. The control group consisted of 25 males and 25

females, and a median age of 53 that ranged from 4 to 90 (1st decade: 3, 2nd decade: 3, 3rd decade: 7, 4th decade: 6, 5th decade: 5, 6th decade: 4, 7th decade: 7, 8th decade: 5, 9th decade: 10, and 10th decade: 1).

Imaging sequences

The cases we retrospectively evaluated were scanned on a 1.5 T clinical scanner (MAGNETOM Avanto, Siemens Healthcare GmbH, Erlangen, Germany with the operating system “syngo MR VB19”). Since the cases were enrolled from routine clinical studies, the image sets were the usual clinical protocols, which included axial fluid attenuated inversion recovery (FLAIR) images (TR/TE/TI=9000 ms/102 ms/2500 ms), coronal T2-weighted images (TR/TE=3800 ms/95 ms) as well as DWIs (Fig. 1). The DWI was scanned with the following parameters: TR = 3500 ms, TE = 94 ms, EPI factor=192, echo spacing = 1.01 ms, bandwidth = 1132 Hz/Px, FOV = 200 mm, 192×144 , 20 slices with distant factor = 20%, slice thickness = 6 mm, averages = 4, acceleration factor = 2, acquisition time = 1 min 50 s, motion proving gradient: bipolar type, b value = 0, 500, 1000 s/mm^2 , 3-scan trace, fat suppression, no flow compensation.

Image analysis

Evaluation of the signal intensity and signal void of CSF on the $b = 500 \text{ s/mm}^2$ DWI

All images were interpreted by a consensus of two neurologists (S.N. and T.T.). We evaluated the signal intensity of the CSF within the ventricle and on the surface of the cerebral sulci, on the $b = 500 \text{ s/mm}^2$ DWI (Figs. 2, 3). The signal intensity of the CSF within the ventricles was evaluated qualitatively in comparison with the white matter signal intensity in the lateral (anterior horn, body, atrium, and temporal horn), 3rd and 4th ventricles. No signal intensity, signal intensity lower than that of white matter, signal intensity equal to white matter, and signal intensity higher than that of white matter were scored as 0, 1, 2, and 3, respectively.

The signal intensity of the CSF in the cerebral surface and ventricular connections was evaluated for the presence of a signal void. In the Sylvian fissure, no signal void, signal void limited to the Sylvian vallicula, signal void until the Sylvian stem, and signal void in the whole Sylvian fissure were scored as 0, 1, 2, and 3, respectively. In the frontoparietal cerebral sulci, no signal void, signal void in one sulcus, signal void in two sulci, and signal void in more than three sulci as 0 and 1, 2, and 3, respectively. For the foramen of Monroe and aqueduct, no signal void, signal void in 1 slice, and signal void more than 2 slices were scored as 0, 1, and 2, respectively.

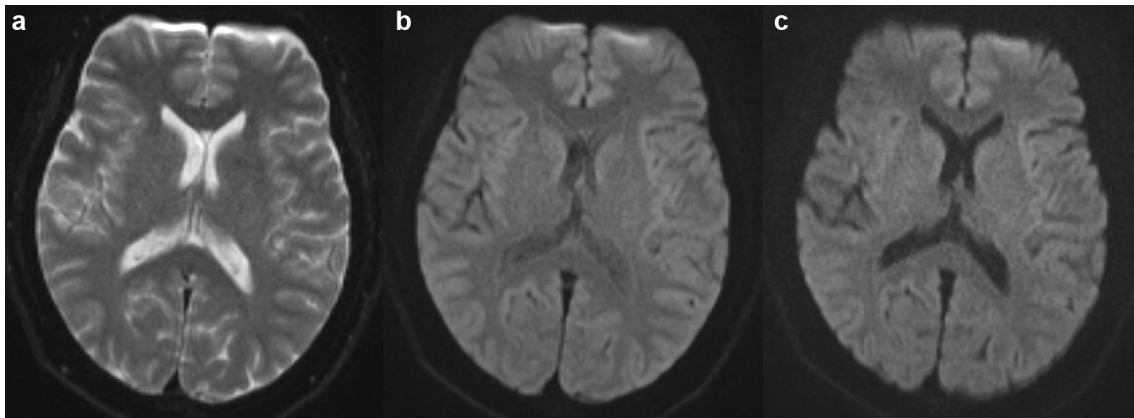


Fig. 1 Diffusion-weighted image with $b=0$ (a), 500 (b) and 1000 s/mm^2 (c). DWIs using multiple b values have been used to obtain accurate ADC values that are insensitive to perfusion effects. Generally, $b=1000 s/mm^2$ is used in clinical practice such as for the detec-

tion of acute infarction. On the $b=500 s/mm^2$ DWI, the signal suppression of the CSF is incomplete, which may give information on the dynamics of CSF

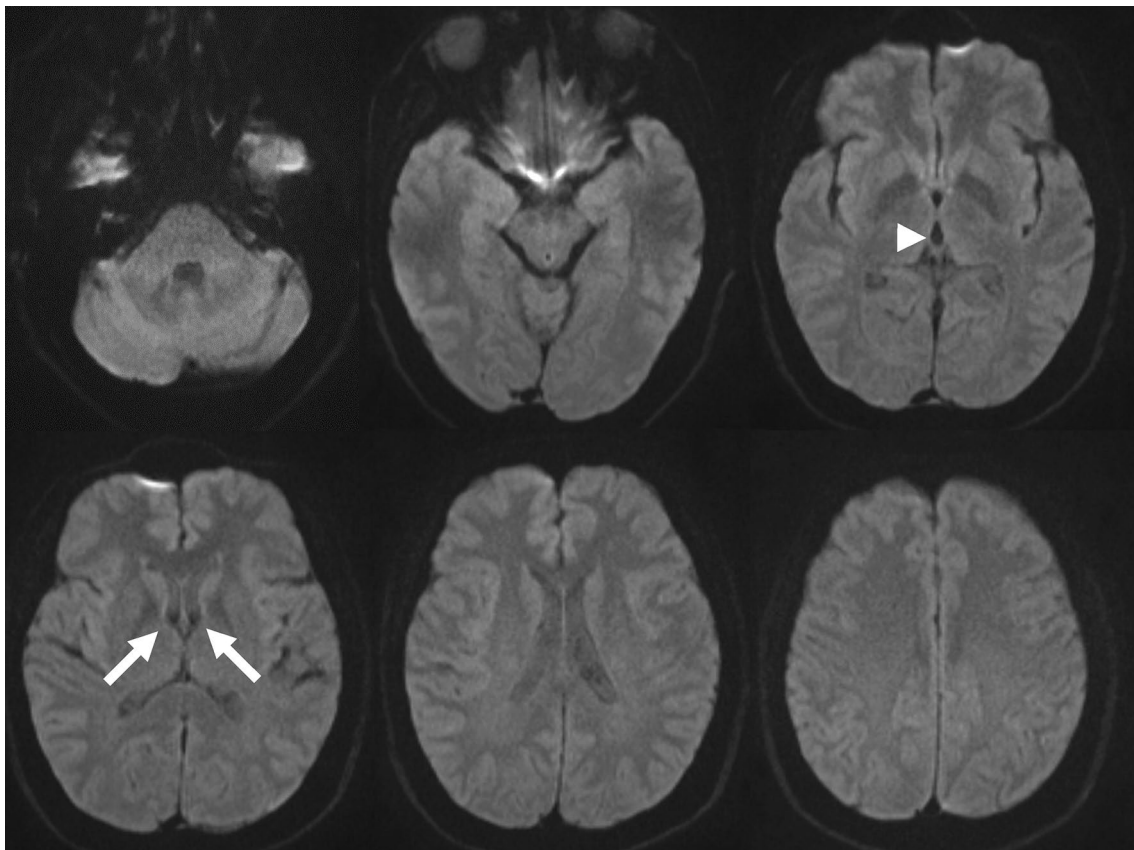


Fig. 2 Control case (60-year-old female) on the $b=500 s/mm^2$ DWI. In general, the CSF within the ventricle had a higher signal intensity compared to the Sylvian fissure. However, signal void from the fora-

men of Monroe (arrows) and aqueduct (arrowhead) is prominent. The low signal intensity within the Sylvian fissure is limited to the horizontal, anterior ascending rami and lower area of the posterior rami

Evaluation of the signal void adjacent to the septum pellucidum on the $b=500 s/mm^2$ DWI

On the $b=500 s/mm^2$ DWI, we evaluated the presence and degree of signal void adjacent to the septum

pellucidum. For the thickness of the signal void, no signal void, signal void with a thickness < 10 mm, and signal void with a thickness ≥ 10 mm were scored as 0, 1, and 2, respectively. For the length of the signal void, no signal void, signal void in part of the septum pellucidum, and

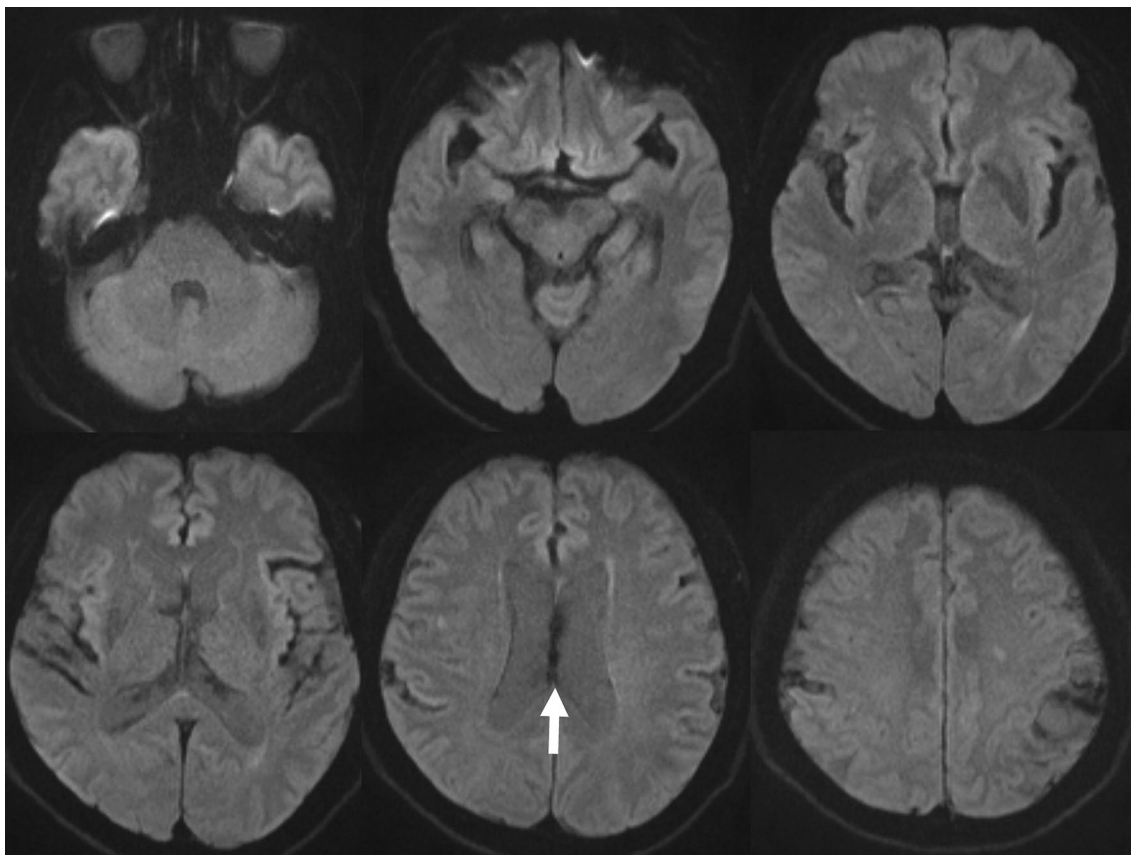


Fig. 3 Ventricular dilatation case (76-year-old male) on the $b=500$ s/mm² DWI. The CSF within the ventricle had a higher signal intensity compared to the control (Fig. 2). The signal void at the foramen of Monroe and aqueduct is less prominent. The low signal intensity

within the Sylvian fissure can be seen in a wide area. The CSF in the cortical sulci in the fronto-parietal area also has a low signal intensity. The characteristic bead-like signal void along the septum pellucidum is indicated (arrow)

signal void in the whole septum pellucidum were scored as 0, 1, and 2, respectively. For the shape of the signal void, no signal void, a thin band-like signal void, and a signal void with a bead-like shape were scored as 0, 1, and 2, respectively. The summation of the three scores was used as total score for signal void adjacent to the septum pellucidum.

Evaluation of the findings related to ventricular dilatation

On axial FLAIR and coronal T2-weighted images, we evaluated the degree and character of the ventricular dilatation. In addition to the Evans index, which is a simple and widely accepted index for ventricular dilatation, we evaluated the findings related to iNPH according to the methods proposed by Kockum et al. as follows [12].

- (a) Evans' index: the ratio between the maximum width of the frontal horns of the lateral ventricles and the maximum inner diameter of the cranium in the same transverse slice [13]. An Evans' index ≤ 0.25 , > 0.25 to 0.3 and > 0.3 was scored as 0, 1, and 2, respectively.
- (b) The narrow parietal high convexity and medial parafalcine sulci were accessed on the coronal plane [14]. Normal, narrowing in the parafalcine area, and a narrowing in the vertices were scored as 0, 1, and 2, respectively.
- (c) Dilation of the Sylvian fissures in the coronal plane was compared to the surrounding sulci [15]. Normal and enlarged were scored as 0 and 1.
- (d) Focally enlarged sulci were defined by comparing them to the surrounding sulci [16]. Normal and enlarged sulci were scored as 0 and 1.
- (e) The diameter of the temporal horns was measured in the transverse plane and the mean width of the right and left sides was calculated [17]. Diameter < 4 mm,

4 to < 6 mm and ≥ 6 mm were scored as 0, 1, and 2, respectively.

- (f) The callosal angle was measured between the lateral ventricles in the coronal plane, through the posterior commissure perpendicular to the anterior–posterior commissural plane [18]. Callosal angles $> 90^\circ$, $90\text{--}60^\circ$, and $\leq 60^\circ$ were scored as 0, 1, and 2, respectively.
- (g) The periventricular white matter hyperintensity along the lateral ventricles was graded according to Fazekas' scale [19]. An absence of hyperintensity, “caps”, or pencil-thin lining, a smooth “halo”, and an irregular PVH extending into the deep white matter, was scored as 0, 1, 2, and 3, respectively.

The total score for the likelihood of iNPH was calculated as a summation of the seven scores with a correction for the total number of scores. Thus, the total score was “score a”/3 + “score b”/3 + “score c”/2 + “score d”/2 + “score e”/3 + “score f”/3 + “score g”/4.

Statistical analysis

Analysis of the signal intensity of CSF on the $b = 500$ s/mm² DWI

Scores for the CSF signal intensity on the $b = 500$ s/mm² DWI were compared between the ventricular dilatation group and controls using a Pearson's Chi-square test. Comparisons were made of the scores for CSF signal intensity in (1) anterior horn of the lateral ventricle, (2) body of the lateral ventricle, (3) atrium of the lateral ventricle, (4) temporal horn of the lateral ventricle, (5) 3rd ventricle, and (5) 4th ventricle. In addition, (6) scores for the signal void in the Sylvian fissure and (7) scores for the signal void in the fronto-parietal cerebral sulci were also compared between groups. We also evaluated the correlation between age and the score listed above within the ventricular dilatation and control groups using a Spearman's correlation coefficient. The calculations were performed with “R” (ver. 3.4.3) (R Development Core Team) [20].

Analysis of the signal void adjacent to the septum pellucidum on the $b = 500$ s/mm² DWI

Scores for the signal void adjacent to the septum pellucidum on the $b = 500$ s/mm² DWI were compared between the ventricular dilatation and control groups using a Pearson's Chi-square test. Comparisons were made for: (1) thickness of the signal void; (2) length of the signal void; and (3) shape of the signal void. We also evaluated the correlation between age and the scores listed above within the two groups using a Spearman's correlation coefficient.

Comparisons of the findings related to ventricular dilatation and the signal void adjacent to the septum pellucidum on the $b = 500$ s/mm² DWI

We compared the findings related to ventricular dilatation and the signal void adjacent to the septum pellucidum on the $b = 500$ s/mm² DWIs of the two groups using a Spearman's correlation coefficient. Following comparisons were made: (1) We compared the total score related to ventricular dilatation, which included findings related to iNPH and the total score for the signal void adjacent to the septum pellucidum on the $b = 500$ s/mm² DWIs. (2) We compared the Evans' index and the total score for the signal void adjacent to the septum pellucidum on the $b = 500$ s/mm² DWIs, to evaluate if the findings were related to iNPH or just to ventricular dilatation.

Results

Analysis of the signal intensity of CSF on the $b = 500$ s/mm² DWI

Table 1 shows the comparisons of CSF signal intensity on the $b = 500$ s/mm² DWI between the ventricle dilatation and control groups by the Pearson's Chi-square test. The scores for CSF signal intensity were significantly higher in the ventricular dilatation group in the anterior horn of the lateral ventricle, the body of the lateral ventricle, the atrium of the lateral ventricle, the temporal horn of the lateral ventricle, and in the 3rd ventricle. However, there was no significant difference in the 4th ventricle. The scores for the signal void in the Sylvian fissure were significantly higher in the ventricular dilatation group, indicating that the signal void occupied a larger area. There were no significant differences for the signal void in the fronto-parietal cerebral sulci. In the ventricular connections including foramen of Monroe and aqueduct, the scores were significantly difference between ventricular dilatation group and control.

Table 2 shows the correlation between age and the scores of the ventricular dilatation and control groups using a Spearman's correlation coefficient. In the control group, the score for the signal void in the Sylvian fissure had a significantly positive correlation with age ($p < 0.05$). However, other scores were not significantly correlated with age.

Analysis of the signal void adjacent to the septum pellucidum on the $b = 500$ s/mm² DWI

Table 3 indicates the comparison of scores for the signal void adjacent to the septum pellucidum on the $b = 500$ s/mm² DWIs between the ventricular dilatation and control groups using a Pearson's Chi-square test. The ventricular dilatation

Table 1 Comparison of scores for CSF signal intensity or signal void between the ventricle dilatation group and controls

| | Score | 0 | 1 | 2 | 3 | Significance | <i>p</i> value |
|---|------------|----|----|----|----|------------------|-------------------------|
| Anterior horn of lateral ventricle | Control | 4 | 42 | 5 | 0 | <i>p</i> < 0.01 | 4.17 × 10 ⁻³ |
| | Dilatation | 0 | 32 | 18 | 1 | | |
| Body of lateral ventricle | Control | 0 | 46 | 5 | 0 | <i>p</i> < 0.05 | 1.07 × 10 ⁻² |
| | Dilatation | 0 | 32 | 17 | 2 | | |
| Atrium of lateral ventricle | Control | 1 | 45 | 5 | 0 | <i>p</i> < 0.01 | 9.01 × 10 ⁻³ |
| | Dilatation | 0 | 31 | 18 | 2 | | |
| Temporal horn of lateral ventricle | Control | 28 | 23 | 0 | 0 | <i>p</i> < 0.001 | 1.94 × 10 ⁻⁶ |
| | Dilatation | 4 | 44 | 3 | 0 | | |
| 3rd ventricle | Control | 40 | 11 | 0 | 0 | <i>p</i> < 0.001 | 8.41 × 10 ⁻⁴ |
| | Dilatation | 20 | 31 | 0 | 0 | | |
| 4th ventricle | Control | 29 | 22 | 0 | 0 | NS | 4.60 × 10 ⁻¹ |
| | Dilatation | 28 | 21 | 2 | 0 | | |
| Signal void in the Sylvian fissure | Control | 0 | 0 | 32 | 19 | <i>p</i> < 0.05 | 3.05 × 10 ⁻² |
| | Dilatation | 0 | 6 | 25 | 20 | | |
| Signal void in the fronto-parietal cerebral sulci | Control | 38 | 1 | 5 | 7 | NS | 3.62 × 10 ⁻¹ |
| | Dilatation | 41 | 2 | 6 | 2 | | |
| Signal void in the foramen of Monroe | Control | 0 | 51 | 0 | | <i>p</i> < 0.001 | 7.28 × 10 ⁻⁶ |
| | Dilatation | 7 | 35 | 9 | | | |
| Signal void in the aqueduct | Control | 0 | 46 | 5 | | <i>p</i> < 0.001 | 1.42 × 10 ⁻⁴ |
| | Dilatation | 11 | 32 | 8 | | | |

Table 2 Correlation between age and CSF signal intensity in the ventricle dilatation group and controls

| | | Spearman's rank correlation coefficient | Significance |
|---|------------|---|-----------------|
| Anterior horn of lateral ventricle | Control | 0.36 | NS |
| | Dilatation | -0.07 | NS |
| Body of lateral ventricle | Control | 0.09 | NS |
| | Dilatation | -0.14 | NS |
| Atrium of lateral ventricle | Control | 0.09 | NS |
| | Dilatation | -0.09 | NS |
| Temporal horn of lateral ventricle | Control | -0.05 | NS |
| | Dilatation | 0.05 | NS |
| 3rd ventricle | Control | 0.16 | NS |
| | Dilatation | 0.20 | NS |
| 4th ventricle | Control | 0.04 | NS |
| | Dilatation | -0.05 | NS |
| Signal void in the Sylvian fissure | Control | 0.68 | <i>p</i> < 0.05 |
| | Dilatation | 0.56 | NS |
| Signal void in the fronto-parietal cerebral sulci | Control | 0.55 | NS |
| | Dilatation | 0.37 | NS |

Table 3 Signal void adjacent to the septum pellucidum on the *b* = 500 s/mm² DWI

| | Score | 0 | 1 | 2 | Significance | <i>p</i> value |
|--------|------------|----|----|----|------------------|--------------------------|
| Width | Control | 40 | 11 | 0 | <i>p</i> < 0.001 | 6.72 × 10 ⁻¹⁵ |
| | Dilatation | 3 | 38 | 10 | | |
| Length | Control | 40 | 11 | 0 | <i>p</i> < 0.001 | 4.51 × 10 ⁻¹⁷ |
| | Dilatation | 3 | 23 | 25 | | |
| Shape | Control | 40 | 10 | 1 | <i>p</i> < 0.001 | 9.25 × 10 ⁻¹⁸ |
| | Dilatation | 3 | 12 | 36 | | |

group had significantly higher scores compared to controls in the thickness ($p < 0.001$), the length ($p < 0.001$), and the shape of the signal void ($p < 0.001$).

Table 4 shows the correlation between age and the scores of the ventricular dilatation and control groups using a Spearman's correlation coefficient. There were no significant correlations with age.

Comparison between ventricular dilatation and the signal void adjacent to the septum pellucidum on the $b = 500 \text{ s/mm}^2$ DWI

Table 5 shows correlation between ventricular dilatation and the signal void adjacent to the septum pellucidum. The total score for ventricular dilatation, which included the findings related to iNPH, was significantly correlated with the total score for the signal void adjacent to the septum pellucidum. In particular, the correlation between the Evans' index and the total score for the signal void adjacent to the septum pellucidum was of greater significance compared to the other scores related to iNPH.

Discussion

The dynamics of cerebrospinal fluid have long been discussed. In classical theory, the CSF is produced actively in the choroid plexus within the ventricle and flows out to be absorbed via the arachnoid villi on the surface of the cranium. The choroid plexus is considered to act as a pump system for the CSF. However, the mechanism for CSF dynamics

is not fully understood and there are controversies. Although it has been believed that CSF is mainly produced in the choroid plexus for a long time, recent studies show negative evidence for this theory and indicate that the choroid plexus may not be the main site of CSF production. Various processes including parenchymal capillaries and arterial hydrostatic pressure differences may play a role in CSF production [21–23]. For absorption of CSF, the arachnoid villi were believed to be the predominant outflow route of CSF in the classical theory. However, recent evidence indicates that the arachnoid villi may not be the primary site of absorption. Instead, other processes including lymphatic outflow and venous osmotic pressure differences have been shown to be more dominant for CSF absorption [22, 24]. To explore CSF dynamics, a variety of methods have been applied [25, 26]. Myelography using iodine contrast media as an extrinsic tracer is one classic method. However, extrinsic tracers such as iodine contrast media have a large molecular weight and their behavior may be different from that of CSF. To investigate CSF dynamics without the use of an extrinsic tracer, a technique called Time-Spatial Labeling Inversion Pulse (Time-SLIP) was developed, which uses spin labeling of CSF itself to visualize motion [27]. Another technique recently applied to evaluate CSF dynamics is four-dimensional velocity mapping (4D-VM or 4D-flow) which is based on a phase contrast technique and provides a quantitative spatiotemporal velocity distribution of CSF motion during a cardiac cycle as vector cine images [28]. In this study, we investigated the use of low b value diffusion-weighted images to evaluate CSF dynamics in a retrospectively selected population with and without ventricular dilatation.

The findings of the current study indicate that CSF within the lateral ventricle on the $b = 500 \text{ s/mm}^2$ DWI had a higher signal intensity in the ventricle dilatation group compared to controls. It is well known that diffusion-weighted images visualize the microscopic motion of water, which includes water molecular diffusion in tissue and microcirculation in the capillary network of tissues [29]. The signal intensity of a diffusion-weighted image depends mainly on the relaxation time, proton density, intra-voxel diffusion, and perfusion. In CSF, the perfusion fraction may correspond to CSF flow. While static protons increase the signal intensity on a diffusion-weighted image, moving protons such as those found in CSF, result in a signal decrease, which is greater

Table 4 Correlation between age and the signal void adjacent to the septum pellucidum in the ventricle dilatation and control groups

| | | Spearman's rank correlation coefficient | Significance |
|--------|------------|---|--------------|
| Width | Control | 0.49 | NS |
| | Dilatation | 0.10 | NS |
| Length | Control | 0.49 | NS |
| | Dilatation | 0.14 | NS |
| Shape | Control | 0.49 | NS |
| | Dilatation | 0.12 | NS |

Table 5 Correlation between the findings related to ventricular dilatation and the signal void adjacent to the septum pellucidum on the $b = 500 \text{ s/mm}^2$ DWIs

| | Spearman's rank correlation coefficient | Significance | p value |
|--|---|--------------|------------------------|
| Total score for the findings related to ventricular dilatation | 0.76 | $p < 0.001$ | 2.24×10^{-14} |
| Score for Evans index | 0.77 | $p < 0.001$ | 4.88×10^{-15} |
| Scores other than Evans index | 0.75 | $p < 0.001$ | 4.31×10^{-14} |

when the flow is faster or when the b value is larger. When the $b = 1000 \text{ s/mm}^2$ MPG is used, the signal intensity of the CSF on a DWI is suppressed significantly. However, when the MPG is lower such as $b = 500 \text{ s/mm}^2$, the signal of the CSF is not suppressed completely, in particular the portion of the signal from static protons in the CSF, that is the basis of the “T2 shine through” phenomenon. Therefore, our finding that the signal intensity of the CSF within the ventricle was higher in the cases with ventricular dilatation means that the motion of the water molecules is slower compared to that of controls.

We did not find a significant correlation between the age and the signal intensity of the CSF on the $b = 500 \text{ s/mm}^2$ DWI other than in the signal void in the Sylvian fissure. However, within the control group, four cases had a very low signal intensity (grade 0) in the anterior horn of the lateral ventricle, and all four cases were younger than 15 years. There were no cases higher than grade 0 in that age range. Conversely, there were five cases that had a signal intensity equal to white matter (grade 2) in the body of the lateral ventricle, and all five were older than 70 years. These findings, although not statistically significant, suggest that the motion of the water molecules within the ventricles also tends to decrease with age.

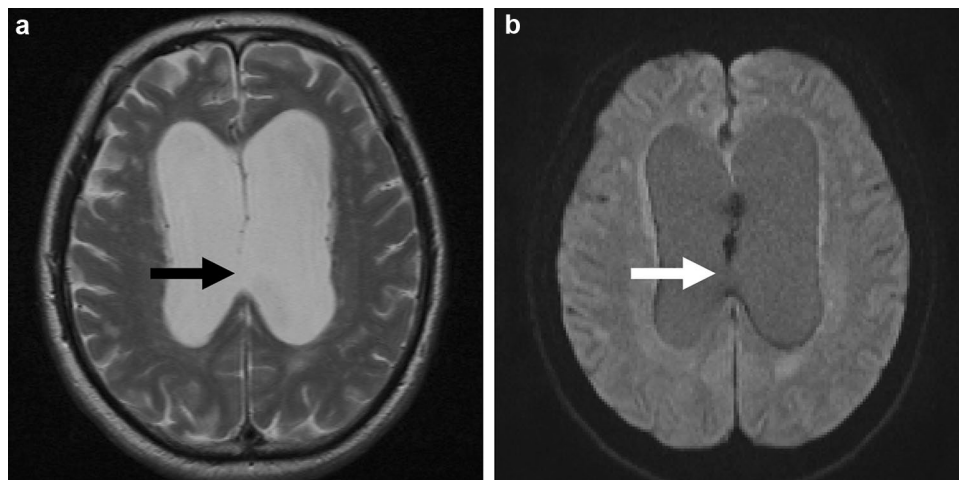
The most interesting or curious finding in the current study may be the characteristic signal void along the septum pellucidum that was found mainly in the ventricular dilatation cases. This finding was significantly correlated with both the Evans’ index and the score for the likelihood of iNPH. There were two patterns of the signal void along the septum pellucidum. One was a rather thin band-like pattern and the other was thicker and bead-like. The thin band-like pattern seemed to appear in the cases with less severe ventricular dilatation and the bead-like pattern in the cases with greater ventricular dilatation. It is interesting to note that in the cases with fenestration in the septum pellucidum due to severe hydrocephalus, the signal void along the septum

pellucidum was not observed near the fenestration (Fig. 4). The total scores of the signal void along the septum pellucidum were significantly correlated with the total score for ventricular dilatation, the score for the Evans’ index, and the other scores related to iNPH. The score for the Evans’ index was more significant compared to the other scores related to iNPH. Thus, the finding may be more likely to be correlated with ventricular dilatation itself than the finding related to iNPH.

We could not determine the source of the signal void along the septum pellucidum in the current study. One speculation is that it is due to flow or jet. However, as mentioned above, in the cases with perforation of the septum pellucidum, the signal void could be seen in the area of the septum, and could not be seen in the area of the septal defect (Fig. 4). In addition, the bead-like signal void was more frequently seen in the cases with a greater degree of ventricular dilatation. With ventricular dilatation, the septum pellucidum becomes thinner [30] and may behave as a drum membrane, where exposure to vibration may cause standing waves. A source of the vibration could be arterial pulsation; however, the septum pellucidum does not contain a large artery. We speculated the vibration of the table of MR scanner, while scanning may be a source, and performed a phantom experiment with a plastic membrane which does not make vibration or pulsation itself. Figure 5 shows images of the phantom experiment with the same imaging sequence as applied in the current study. On the DWI (Figure 5b), there is a bead-like signal void along the plastic membrane from which the vibration was only due to the scanning of the DWI sequence. Of course, this phenomenon may not be identical to the signal void along the septum pellucidum. The standing wave produced by mechanical vibration of the bed from scanning sequence may be one of the causes of the bead-like signal void.

The low b value DWI in the current study is not specially designed for evaluating CSF dynamics. Therefore,

Fig. 4 A case with perforation in the septum pellucidum. A case with ventricular dilatation and perforation in the posterior part of the septum pellucidum (arrow in **a**: T2-weighted image). The bead-like signal void can be seen in the area where the septum present. In contrast, the signal void is not seen in the area of the septal defect (arrow in **b**: $b = 500 \text{ s/mm}^2$ DWI)



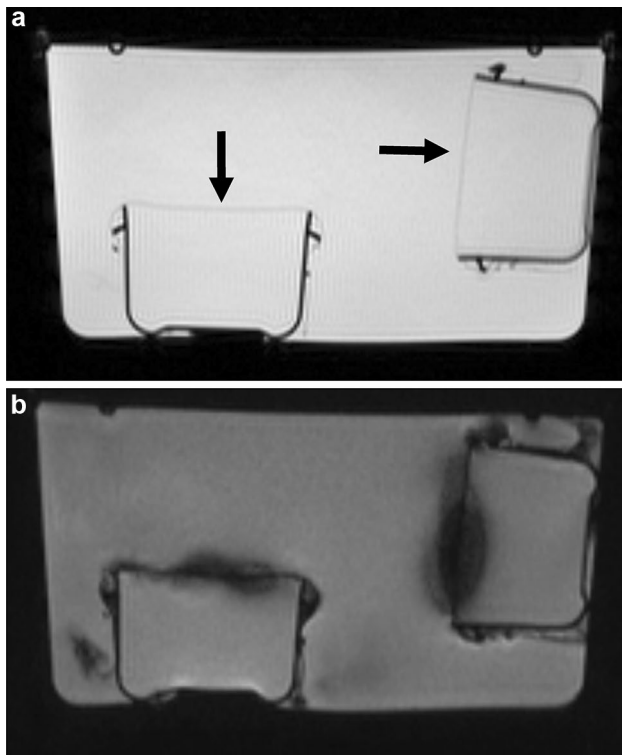


Fig. 5 Phantom study (for reference). We created a phantom in which plastic membranes (0.08 mm thickness) were mounted within water. A half-Fourier single-shot turbo spin echo (HASTE) image (a) shows the structure of the phantom and indicates the location of the plastic membranes (arrows). A low b value DWI identical to the clinical scan was applied to this phantom (b), which showed like a signal void along the plastic membrane. Of course, this phenomenon may not be identical to the signal void along the septum pellucidum. We speculate that the standing wave produced by vibration of the scanner bed from the DWI scanning may account for the observed signal void on the low b value DWI

this imaging sequence cannot evaluate the direction of the flow and cannot provide quantitative information on the CSF dynamics. Thus, the findings on low b value DWI is a kind of indirect information compared to specially designed methods such as Time-SLIP or 4D-flow. However, the current study showed that it may reflect changes of CSF dynamics in the cases with ventricular dilatation. Although the information provided by the low b value DWI in the current study is not optimal for the evaluation of CSF dynamics, there would be several advantages for this imaging. The short acquisition time of the low b value DWI is one advantage. The acquisition time of the sequence we used was 1 min and 50 s including the $b = 1000$ image. Since the 4D-flow method uses cardiac gating, the acquisition time tends to be long for coverage of the whole brain. Whole brain coverage is also an advantage of our method. The Time-SLIP method can sample only one region of the brain in a single scan. Thus, the

low b value DWI might be used as a quick and convenient technique to get gross information on CSF dynamics. The major disadvantage of this technique is the lack of spatial and temporal quantification. It may be possible to calculate a perfusion-related diffusion coefficient (D^*) from the signal of the $b = 0$ and $b = 500$ s/mm² images [31]. However, the signal intensity varies by the design of the MPG or other imaging parameters. It has been reported that CSF pulsation artifacts on ADC maps can be affected by the number of readout segments [32]. We used a scoring method instead of signal value measurement to evaluate the signal characteristics in this retrospective study to avoid influence from the above-mentioned factors.

This study has several limitations. First, the study was designed as a retrospective study using clinically obtained images, which were not designed specifically for the evaluation of hydrocephalus. Case selection in the current study is based on the description of the clinical reports thus not optimally randomized ones. Second limitation is lack of optimization of the sequence especially in the b value. The b value of 500 s/mm² is not optimized for the evaluation of CSF dynamics but just for the calculation of ADC values. Therefore, optimization of the b value will be needed in the further study. Another limitation is the lack of clinical evidence for the cause of the hydrocephalus. Although we classified cases into ventricular dilatation and controls, both groups contained various underlying conditions. To compensate for this limitation, we evaluated factors relating to ventricular dilatation including the Evans' index, narrowed parietal high convexity, dilation of the Sylvian fissures, focally enlarged sulci, callosal angle or periventricular white matter hyperintensity to characterize the ventricular dilatation. A lack of follow up may be another limitation of this study and may be explored in a future investigation.

In conclusion, we retrospectively evaluated the $b = 500$ s/mm² diffusion image obtained in routine clinical practice for correlation to CSF dynamics and found that the signal intensity of the $b = 500$ s/mm² diffusion image may reflect changes in CSF dynamics. Although this method cannot quantify the absolute flow speed, it might be possible to evaluate the distribution of altered CSF dynamics within the cranium in the cases of ventricular dilatation. A characteristic bead-like signal void along the septum pellucidum could be seen in the cases with ventricular dilatation, which was speculated to be due to a standing wave in a thinned septum pellucidum. However, the current study is a retrospectively designed preliminary study, and further studies including optimization of the sequence, comparison with other method such as Time-SLIP or 4D-flow method, and the study with case randomization will be needed.

Compliance with ethical standards

Conflict of interest One of the authors is an employee of Siemens Japan K.K.

Ethical statement All applicable institutional and/or national guidelines for care were followed.

References

1. Taoka T, Masutani Y, Kawai H, Nakane T, Matsuoka K, Yasuno F, et al. Evaluation of glymphatic system activity with the diffusion MR technique: diffusion tensor image analysis along the perivascular space (DTI-ALPS) in Alzheimer's disease cases. *Jpn J Radiol*. 2017;35(4):172–8.
2. Sparacia G, Cannella R, Lo Re V, Mamone G, Sakai K, Yamada K, et al. Brain-core temperature of patients before and after orthotopic liver transplantation assessed by DWI thermometry. *Jpn J Radiol*. 2018;36(5):324–30.
3. Xu XQ, Wu CJ, Zu QQ, Lu SS, Liu XL, Gao QQ, et al. Temporal evolution of the signal intensity of hyper-acute ischemic lesions in a canine stroke model: influence of hyperintense acute reperfusion marker. *Jpn J Radiol*. 2017;35(4):161–7.
4. Hori M, Fukunaga I, Masutani Y, Taoka T, Kamagata K, Suzuki Y, et al. Visualizing non-Gaussian diffusion: clinical application of q-space imaging and diffusional kurtosis imaging of the brain and spine. *Magn Reson Med Sci*. 2012;11(4):221–33.
5. Kanda T, Wakabayashi Y, Zeng F, Ueno Y, Sofue K, Maeda T, et al. Imaging findings in radiation therapy complications of the central nervous system. *Jpn J Radiol*. 2018;36(9):519–527.
6. Zitouni S, Koc G, Doganay S, Saracoglu S, Gumus KZ, Ciraci S, et al. Apparent diffusion coefficient in differentiation of pediatric posterior fossa tumors. *Jpn J Radiol*. 2017;35(8):448–53.
7. Tachibana Y, Aida N, Niwa T, Nozawa K, Kusagiri K, Mori K, et al. Analysis of multiple B-value diffusion-weighted imaging in pediatric acute encephalopathy. *PLoS One*. 2014;8(6):e63869.
8. Naganawa S, Sato K, Katagiri T, Mimura T, Ishigaki T. Regional ADC values of the normal brain: differences due to age, gender, and laterality. *Eur Radiol*. 2003;13(1):6–11.
9. Le Bihan D, Breton E, Lallemand D, Grenier P, Cabanis E, Laval-Jeantet M. MR imaging of intravoxel incoherent motions: application to diffusion and perfusion in neurologic disorders. *Radiology*. 1986;161(2):401–7.
10. Fujima N, Sakashita T, Homma A, Yoshida D, Kudo K, Shirato H. Utility of a hybrid IVIM-DKI model to predict the development of distant metastasis in head and neck squamous cell carcinoma patients. *Magn Reson Med Sci*. 2018;17(1):21–7.
11. Urushihata T, Takuwa H, Seki C, Tachibana Y, Takahashi M, Kershaw J, et al. Water diffusion in the brain of chronic hypoperfusion model mice: a study considering the effect of blood flow. *Magn Reson Med Sci*. 2018;17(4):318–324.
12. Kockum K, Lilja-Lund O, Larsson EM, Rosell M, Soderstrom L, Virhammar J, et al. The iNPH Radscale; a radiological scale for structured evaluation of idiopathic normal pressure hydrocephalus. *Eur J Neurol*. 2018;25(3):569–576.
13. Evans WA Jr. An encephalographic ratio for estimating ventricular enlargement and cerebral atrophy. *Arch Neurol Psychiatry*. 1942;47(6):931–7.
14. Sasaki M, Honda S, Yuasa T, Iwamura A, Shibata E, Ohba H. Narrow CSF space at high convexity and high midline areas in idiopathic normal pressure hydrocephalus detected by axial and coronal MRI. *Neuroradiology*. 2008;50(2):117–22.
15. Kitagaki H, Mori E, Ishii K, Yamaji S, Hirono N, Imamura T. CSF spaces in idiopathic normal pressure hydrocephalus: morphology and volumetry. *AJNR Am J Neuroradiol*. 1998;19(7):1277–84.
16. Holodny AI, George AE, de Leon MJ, Golomb J, Kalnin AJ, Cooper PR. Focal dilation and paradoxical collapse of cortical fissures and sulci in patients with normal-pressure hydrocephalus. *J Neurosurg*. 1998;89(5):742–7.
17. Virhammar J, Laurell K, Cesarini KG, Larsson EM. Preoperative prognostic value of MRI findings in 108 patients with idiopathic normal pressure hydrocephalus. *AJNR Am J Neuroradiol*. 2014;35(12):2311–8.
18. Ishii K, Kanda T, Harada A, Miyamoto N, Kawaguchi T, Shimada K, et al. Clinical impact of the callosal angle in the diagnosis of idiopathic normal pressure hydrocephalus. *Eur Radiol*. 2008;18(11):2678–83.
19. Fazekas F, Chawluk JB, Alavi A, Hurtig HI, Zimmerman RAMR. Signal abnormalities at 1.5 T in Alzheimer's dementia and normal aging. *Am J Neuroradiol*. 1987;8(3):421–6.
20. Ihaka R, Gentleman R. R: a language for data analysis and graphics. *J Comput Graph Stat*. 1996;5:299–314.
21. Naganawa S, Nakane T, Kawai H, Taoka T. Gd-based contrast enhancement of the perivascular spaces in the basal ganglia. *Magn Reson Med Sci*. 2017;16(1):61–5.
22. Miyajima M, Arai H. Evaluation of the production and absorption of cerebrospinal fluid. *Neurol Med Chir (Tokyo)*. 2015;55(8):647–56.
23. Oreskovic D, Rados M, Klarica M. Role of choroid plexus in cerebrospinal fluid hydrodynamics. *Neuroscience*. 2017;354:69–87.
24. Taoka T, Naganawa S. Gadolinium-based contrast media, cerebrospinal fluid and the glymphatic system: possible mechanisms for the deposition of gadolinium in the brain. *Magn Reson Med Sci*. 2018;17(2):111–9.
25. Taoka T, Yamada S, Sakamoto M, Akashi T, Miyasaka T, Ochi T, et al. Accuracy for predicting adhesion between meningioma and the brain by using brain surface motion imaging: comparison between single and double acquisition methods. *Neuroradiology*. 2012;54(12):1313–20.
26. Taoka T, Yamada S, Yamatani Y, Akashi T, Miyasaka T, Emura T, et al. Brain surface motion imaging to predict adhesions between meningiomas and the brain surface. *Neuroradiology*. 2010;52(11):1003–10.
27. Yamada S, Miyazaki M, Kanazawa H, Higashi M, Morohoshi Y, Bluml S, et al. Visualization of cerebrospinal fluid movement with spin labeling at MR imaging: preliminary results in normal and pathophysiologic conditions. *Radiology*. 2008;249(2):644–52.
28. Yatsushiro S, Sunohara S, Hayashi N, Hirayama A, Matsumae M, Atsumi H, et al. Cardiac-driven pulsatile motion of intracranial cerebrospinal fluid visualized based on a correlation mapping technique. *Magn Reson Med Sci*. 2018;17(2):151–60.
29. Le Bihan D, Breton E, Lallemand D, Aubin ML, Vignaud J, Laval-Jeantet M. Separation of diffusion and perfusion in intravoxel incoherent motion MR imaging. *Radiology*. 1988;168(2):497–505.
30. Sarwar M. The septum pellucidum: normal and abnormal. *AJNR Am J Neuroradiol*. 1989;10(5):989–1005.
31. Kang KM, Choi SH, Kim DE, Yun TJ, Kim JH, Sohn CH, et al. Application of cardiac gating to improve the reproducibility of intravoxel incoherent motion measurements in the head and neck. *Magn Reson Med Sci*. 2017;16(3):190–202.
32. Ohashi T, Naganawa S, Kanou M, Ikeda M. CSF pulsation artifacts on ADC maps obtained with readout-segmented EPI. *Magn Reson Med Sci*. 2017;16(2):123–8.